HHS Public Access

Author manuscript

J Biomed Mater Res B Appl Biomater. Author manuscript; available in PMC 2020 May 01.

Published in final edited form as:

J Biomed Mater Res B Appl Biomater. 2020 May ; 108(4): 1262–1273. doi:10.1002/jbm.b.34474.

Hot Isostatic Pressure Treatment of 3D Printed Ti6Al4V Alters Surface Modifications and Cellular Response

Michael B. Berger[1], **Thomas W. Jacobs**[1], **Barbara D. Boyan**[1,2], **Zvi Schwartz**[1,3]

[1]Department of Biomedical Engineering, College of Engineering, Virginia Commonwealth University, Richmond VA 23284, USA

[2]Wallace H. Coulter Department of Biomedical Engineering, Georgia Institute of Technology, Atlanta, GA 30332, USA

[3]Department of Periodontics, University of Texas Health Science Center at San Antonio, San Antonio, Texas 78229, USA

Abstract

Additive manufacturing can be used to create personalized orthopaedic and dental implants with varying geometries and porosities meant to mimic morphological properties of bone. These qualities can alleviate stress shielding and increase osseointegration through bone in-growth, but at the expense of reduced fatigue properties compared to machined implants, and potential for loose build particle erosion. Hot isostatic pressure (HIP) treatment is used to increase fatigue resistance; implant surface treatments like grit-blasting and acid-etching create microroughness and reduce the presence of loose particles. However, it is not known how HIP treatment affects surface treatments and osseointegration of the implant to bone. We manufactured two titanium-aluminum-vanadium (Ti6Al4V) constructs, one with simple through-and-through porosity and one possessing complex trabecular bone-like porosity. We observed HIP treatment varied in effect and was dependent on architecture. Micro/meso/nano surface properties generated by grit-blasting and acid-etching were altered on biomimetic HIP-treated constructs. Human mesenchymal stem cells (MSCs) were cultured on constructs fabricated +/− HIP and subsequently surface-treated. MSCs were sensitive to 3D-architecture, exhibiting greater osteogenic differentiation on constructs with complex trabecular bone-like porosity. HIP-treatment did not alter the osteogenic response of MSCs to these constructs. Thus, HIP may provide mechanical and biological advantages during implant osseointegration and function.

Keywords

Titanium; Mesenchymal stem cells; Additive manufacturing; Biomaterials; Hot isostatic pressure; Powder bed laser fusion

Corresponding Author: Barbara D. Boyan, Ph.D., College of Engineering, Virginia Commonwealth University, 601 West Main Street, Richmond, VA 23284-3068, Phone: 804-828-0190, bboyan@vcu.edu.

Author Contributions:

MBB, BDB, ZS planned experiments and interpreted the data. MBB and TWJ conducted experiments. MBB and TWJ analyzed the data. MBB, TWJ, BDB, and ZS prepared the manuscript.

Introduction

Commercially available titanium (Ti) and titanium-aluminum-vanadium (Ti6Al4V) dental and orthopaedic implants have demonstrated high rates of successful implant retention in healthy patients (>90%). However, for patients with compromised metabolic diseases such as osteoporosis or diabetes, implant failures become more prevalent.[1,2] Osteoporosis alone affects 200 million women worldwide and is a leading cause of reduced quality of life in the United States.[3] It is predicted that fracture rates among the older adult population will double to more than 3 million fractures annually by 2025.[4] With increased life expectancy, successfully integrated implants will be required to last longer than the traditional implant lifespans of 15–20 years. Therefore, there is a strong clinical need for the development of new implant technologies with increased longevity and greater integration with natural bone.

Ti6Al4V is an extensively studied biomaterial, used in bone for its superior biocompatibility due to its ability to form a passive oxide layer. Its excellent material properties make Ti6Al4V strong yet light, as well as corrosion resistant, and it possesses a high affinity for bone apposition.[5] Studies have shown that modifying the surface properties of Ti and its alloys to increase micro/meso/nano-scale roughness via grit-blasting and acid-etching and increasing hydrophilicity by reducing exposure to hydrocarbon adsorption, result in enhanced osteoblast response and mesenchymal stem cell (MSC) differentiation.[6–8] These surfaces possess topographic similarities to osteoclast resorption pits and more closely mimic the physical surface of the bone.[9] These physical cues direct differentiation of MSCs into osteoblasts by augmenting their production of osteogenic proteins. Studies show these surfaces increase production of soluble bone morphogenetic protein 2 (BMP2), osteocalcin (OCN), vascular endothelial growth factor (VEGF), and transforming growth factor beta 1 (TGFβ1), which are desired in an osteogenic environment. Additionally, implants demonstrated to possess osteogenic surface properties in vitro have demonstrated strong implant osseointegration in the clinic. [10–16]

Additive manufacturing (AM) is the process of joining materials in a layer-by-layer fashion to produce a 3-dimensional (3D) object from computer-aided design blueprints and has the potential to provide implants with complex geometries. AM has been used in the aerospace industry for its advanced on-the-spot manufacturing and reduced material waste, thereby reducing costs, increasing efficiency, and allowing new innovative structural design.[17] This manufacturing method has more recently been converted to develop constructs made of titanium and its alloys for dental and orthopaedic applications.[18,19]

Advantages of AM include the ability to alter macro-scale spatial boundary conditions to increase bone-to-implant contact, more closely mimic the mechanical modulus of bone, and promote vascularization needed for net new bone formation.[20] However, for implants that depend on bone ingrowth for stability, there is still debate on the optimal architecture and pore properties for enhanced osseointegration. Porous implants support increased bone in-growth, although a study comparing AM fabricated porous implants with solid implants in rabbit tibial bone defects and in a rat calvarial on-lay model for vertical bone ingrowth, showed that the porous implants were comparable to their solid counterparts concerning pull out force to failure.[21,22] The specific properties of the pores can also affect outcomes.

Studies using a goat femur model have shown that varying pore size can affect early fixation and vascularization.[23]

AM fabrication of Ti6Al4V can result in stress concentrations within the implant due to thermal discrepancies during manufacturing and the existence of imperfections on the exterior of the bulk material that collectively can impair its fatigue characteristics.[24,25] The Standardization Roadmap for Additive Manufacturing Version 2.0 points out that this is also the case for additively manufactured medical implants.[26] While there is a clear need for post-manufacturing modifications to improve durability and mechanical behavior of Ti and Ti alloy implants, little is known about how post-build modifications following hot isostatic pressure (HIP) treatment to reduce stress concentrations within the implant can impact cell response necessary for proper osseointegration.

Post-processing of AM constructs by HIP is conducted to enhance the fatigue resistance of alloyed Ti. Constructs are heat treated in a high-pressure environment to more completely fuse the metallic particles sintered by powder bed laser fusion. The resulting constructs have a reduced micro-porosity within the solid sintered geometry due to a combination of plastic deformation, creep, and diffusion bonding. The heat treatment relaxes stress concentrations by removing intrinsic stresses created during the fusion process and improves the fatigue properties of the finished construct.[24–28] Previous studies have focused and validated the effect of HIP treatment and grit-blasting on solid testing specimens produced by AM by decreasing crack initiation sites through pore removal throughout the cross-section or near the surface, respectively.[25] However, it is not known if HIP treatment alters post-build surface properties like microtopography, which is important for directing cellular response to Ti6Al4V.

The objective of the present study was to evaluate the response of MSCs to 3D porous Ti6Al4V constructs that were produced by AM and then treated with HIP prior to modifying surface properties of the construct. To do this, we fabricated porous Ti6Al4V constructs with two different geometries: a biomimetic architecture based on trabecular bone and an organized geometric shape and treated them with HIP. We further modified the surface of the implants by grit blasting and acid etching. The effects of HIP treatment were examined on the bulk material as well as on surface micro-architecture and these findings were correlated to changes in cellular response. We hypothesized that HIP treatment would not alter the macroscale properties of the implants but microscale/mesoscale properties would be affected. Moreover, laser sintered implants with a three-dimensional, biomimetic porosity and a micro/meso/nano rough surface topography generated after HIP treatment would increase osteoblastic cell response compared to organized geometric laser sintered constructs with the same surface treatments.

Methods

Material Manufacturing

Computer-aided design of biomimetic and organized geometric constructs—

Biomimetic constructs were fabricated as described previously.[19] A computed tomographic (CT) scan was taken of a human femoral head retrieved from a hip replacement

(μCT 40, Scanco Medical, Bassersdorf, Switzerland) with a 16 μm voxel size. A biomimetic template was created using Scanco software (Scanco Medical, Bassersdorf, Switzerland) and rotated and superimposed on itself 24 times. Organized geometric constructs were created by combining cubes 1mm × 1mm with a pore size of 600 microns that were assembled into a cylindrical lattice structure as a control (Materialize Magics, Lueven, Belgium). Generated 3D renderings for both geometries were manufactured into Ti6Al4V circular discs measuring 15mm in diameter by 6mm in height to fit a 24 cell culture well plate.

Powder bed laser fusion—Ti6Al4V (grade 5) particles were purchased from Advanced Powders & Coatings (Quebec, Canada). Ti6Al4V particles 25–45 μm in diameter were produced by plasma atomization and sorted by sieving for ISO 13485 certification for medical devices.

Direct metal laser sintering (DMLS). DMLS was performed using a continuous 200W Ytterbium fiber laser system (EOS, EmbH Munchen, Germany). Laser scanning speed was 7 m s^{-1} with a wavelength of 1054 nm, step size of 100 μm and laser spot size of 0.1 mm.

Hot isostatic pressure treatment—All constructs were removed from the manufacturing plate, and half were treated by hot isostatic pressure (HIP) treatment. Constructs were placed in a pressure vessel furnace and heat treated to 915±14°C at 100 MPa for 120 minutes, to promote α + β grain formation and match studies conducted previously.[25]

Surface treatment—Constructs that do not undergo any additional post-manufacturing modifications can possess partially sintered particles on the implant surface. These remaining microparticles could detach during implant placement, and small particulate of metals are cytotoxic.[29] For this reason, following HIP treatment, constructs were grit-blasted and acid-etched as described previously.[19,30] In brief, constructs first were calcium phosphate grit-blasted using proprietary technology (AB Dental, Ashdod, Israel). Subsequently, constructs were acid-etched by ultrasonication in a 0.3 N nitric acid solution for 5 minutes at 45°C and then rinsed two times in ultrapure water at 25°C for 5 minutes each. Constructs were then rinsed in 97% methanol for 5 minutes before pickling to remove impurities. Pickling treatment consisted of three 10 minute ultrasonic rinses in ultrapure distilled H_2O, followed by submersion in a 1:1 solution of 20 g L^{-1} NaOH and 20 g L^{-1} H_2O_2 for 30 minutes at 80°C, and ultrasonication in ultrapure distilled H_2O for 10 minutes. Constructs were then degreased for 12 minutes, and submerged in 65% aqueous nitric acid at 100°C for 10 minutes, and were finally rinsed 3 times in ultrapure distilled H_2O for 10 minutes. Constructs were then blotted, air dried and sterilized by gamma irradiation before analysis and cell culture.

Material Characterization

Scanning electron microscopy—Surface topography was qualitatively assessed using scanning electron microscopy (SEM; Hitachi SU-70, Tokyo, Japan). Constructs were secured on SEM imaging mounts by carbon tape and imaged with 56 μA ion current, 5 kV accelerating voltage and 5 mm working distance. Five locations per disk were imaged at

each magnification to ensure homogenous assessment, with at least two disks per group imaged.

X-ray photoelectron spectroscopy—X-ray photoelectron spectroscopy (XPS) was used to analyze surface chemistry (PHI VersaProbe III Scanning XPS, Physical Electronics Inc., Chanhassen, MN). Copper clips and instrument mount were sonicated in ethanol for 10 min prior to securing samples. Analysis was conducted using a 50 watt, 15kV x-ray gun with a spot size of 200 μm, 20 ms dwelling time and 1eV step size. Five locations were analyzed per constructs with two constructs per group.

Energy dispersive X-ray spectroscopy

Energy dispersive x-ray spectroscopy (EDX, Hitachi SU-70, Tokyo, Japan) was used to analyze bulk chemistry of the manufactured constructs. An acceleration voltage of 20kV and a sampling time of 60 seconds was used. Peak identification and weight percentage was determined with EDAX Genesis software. Five locations were analyzed per constructs with two constructs per group.

Laser confocal microscopy—Surface roughness was qualitatively assessed by laser confocal microscopy (LCM; Zeiss LSM 710). Z-stacks were obtained with a Plan Apochromat 20x/0.8 M27 objective with a 5x optical zoom, using a 405 nm laser in reflection mode at 50% power. Scan parameters were 0.39 μs pixel dwell, and 25 μm pinhole, 85.02 × 85.02 μm image size, and step size of 1μm. Average surface roughness (Sa) was defined as the average absolute distance in the z-plane; peak to valley distance was defined as the vertical distance between the highest peak and lowest valley for each sample; skewness is the measure of lack of symmetry of a distribution probability and positive skewness is representative of elevations protruding from a relatively flat surface; kurtosis is a measure of the peakedness of the surface and values above 3 are defined as sharp peaks and values below 3 are more rounded [14]. Values were obtained using ZEN software (Zeiss) and shown as the mean and standard error for six samples per group.

Micro-computed tomography—Micro-computed tomography (micro-CT, Skyscan 1173, Bruker, Kontich, Belgium) was used to analyze construct properties. Implants were scanned at a resolution of 1120×1120 pixels, using a brass 0.25 mm filter with a voltage of 100 kV, a current of 80 μA, image pixel scale of 15.1 μm, exposure time of 250 ms and rotation step of 0.2 degrees. A standard Feldkamp reconstruction was performed with a Gaussian smoothing kernel of zero and a beam hardening correction of 20% using NRecon software version 1.6.9.17 (Bruker) and analyzed in CT-Analyser version 1.14.4.1 (Bruker). Constructs were binarized and construct volume, strut thickness and distribution, pore size, open porosity, and closed porosity were calculated within a fixed volume of interest averaged for three constructs per group.

Mechanical Testing

To determine the effects of HIP treatment and different geometries, the compressive modulus, construct toughness, and peak load of the 3D constructs was determined using an MTS Insight 30 electromechanical testing machine (MTS Systems, Minnesota, USA).

Constructs were secured with a preload of 0.01 kN applied at a rate of 0.025 mm s^{-1}. Tests were conducted at a loading rate of 0.02 mm s^{-1} until failure or a maximum load of 30kN. Data collection rate was 500 Hz, and the compressive modulus was calculated as the slope output of the stress/strain curve. Toughness was calculated as the area under the curve, and peak load was measured as the ultimate load point before failure. Tests were carried out on six constructs per group.

Cell Culture

Human MSCs (Lonza Biosciences, Walkersville, MD) were cultured in MSC growth medium (MSCGM; Lonza Biosciences) at 37°C in 5% CO_2 and 100% humidity and cultured to confluence in T75 flasks (Corning Inc., Oneonta, NY) before plating on the constructs. For biological analysis, 3D constructs were placed in a 24-well plate, and cells were plated at a density of 60,000 cells/mL at 1mL per well. 24 hours after plating, constructs were moved to a new well plate and MSCGM were changed with subsequent media changes every 48 hours after that for seven days. On day seven cells were incubated for 24 hours with fresh MSCGM before harvest. At harvest, conditioned media were subsequently collected and stored at −80°C, and MSCs were rinsed twice with 1x PBS, and placed in 1mL of Triton-X100 and stored at −80°C for biological assays.

Biological Response

Cell layers were lysed by ultrasonication at 40V for 15 seconds/well (VCX 130; Vibra-Cell, Newtown, CT). The QuantiFluor* dsDNA system (Promega, Madison, WI) was used to determine total DNA content by fluorescence. Tissue non-specific alkaline phosphatase activity was measured in the cell layer lysates by the release of para-nitrophenol from para-nitrophenyl phosphate (pH 10.2) and normalized to time and protein content measured by bicinchoninic acid assay (Thermo Fisher Scientific, Waltham, MA).

Enzyme-linked immunosorbent assays were used to determine the levels of osteogenic factors in the conditioned media. Osteocalcin (Thermo Fisher), osteoprotegerin (R&D Systems, Inc., Minneapolis, MN), vascular endothelial growth factor A (R&D Systems, Inc.), bone morphogenetic protein 2 (Pepro Tech, Rocky Hill, NJ), interleukin 6 (R&D Systems, Inc.), and interleukin 10 (R&D Systems, Inc.) were quantified according to manufacturer’s protocol.

Statistical Analysis

Data are means ± standard error mean of six independent cultures/variable. All experiments were repeated to ensure the validity of observations, with results from individual experiments shown. Statistical analysis among groups was performed by one-way analysis of variance (ANOVA) and multiple comparisons between the groups were conducted with a two-tailed Tukey correction. A p-value of less than 0.05 was considered statistically significant. All statistical analysis was performed with GraphPad Prism version 5.04.

Data Availability

The data that support the findings of this study are available within the paper. The datasets generated and analyzed during the current study are available from the corresponding author on reasonable request.

Results

HIP treatment affects the physical properties of AM implants.

To test our hypothesis, we generated constructs with two different macro-architectures. Biomimetic constructs were designed to mimic the architecture of trabecular bone found in the femoral head.[19] Geometric constructs were cube unit cells repeated to create a through-and-through geometric lattice. MicroCT assessment of their physical properties showed that the macro-scale geometries were not significantly altered by HIP treatment, for either the biomimetic (Fig. 1a, b) or the geometric (Fig. 1c, d) construct groups. In contrast, cross-sectional images showed distinct differences in geometry, and interconnectivity of the pores between biomimetic and geometric groups.

Closed porosity is a measure of the microvoids or defects within the final AM construct. HIP treatment decreased the presence of microvoids within the biomimetic constructs but did not affect the closed porosity of the geometric constructs and geometric constructs have decreased microvoids compared to biomimetic architectures regardless of HIP treatment (Fig. 2a). Both types of constructs were designed to possess 70% open porosity (Fig. 2b), and a pore size of 600 μm (Fig. 2d). Quantification of the microCT reconstructions confirmed these design parameters. HIP treatment of both types of constructs did not affect construct volume (CV/TV), strut thickness, strut distribution, pore size, open porosity, or total porosity compared to non-HIP treated controls (Fig. 2a–f). However, geometric constructs possessed decreased construct volume, and increased open porosity compared to biomimetic constructs of matching HIP treatment status (Fig. 2b–c).

Architectural differences in design were demonstrated by strut thickness and distribution. These properties are dependent on the volume and distribution of build material within uniform sub-volumes of the manufactured constructs. Strut thickness, defined as the average thickness of structures within a unit volume of space, was 190 μm in the biomimetic constructs regardless of HIP treatment and was increased to roughly 340 μm in the geometric 3D constructs (Fig. 2e). Strut distribution, or the distribution of structures within that same unit volume, was inversely related to strut thickness (Fig. 2f). Open porosity and total porosity were equal, and the interconnectivity for each construct group was greater than 99% (Fig. 2a, b).

Bulk chemistry and surface chemistry are unaffected by HIP treatment.

Bulk chemistry of the Ti6Al4V constructs was determined by EDX. For each group Ti ranged from 89.9 to 91.2 weight percent, aluminum ranged from 7.5 to 8.1 weight percentage, and vanadium ranged from 1 to 1.6 weight percent. No differences were seen between treatment groups. Surface treatment by grit-blasting and acid-etching appears to

decrease the weight percent of vanadium near the implant surface, increasing the weight percent of aluminum (Table 1).

Surface chemistry analysis by XPS demonstrates a similar effect. Vanadium was not detected on the surface of these testing constructs. Oxygen was the highest element present on the implant surface at 55 percent, and was similar between all groups. Carbon was the 2nd most abundance element on the implant surface at 22 percent for all groups. Titanium was the 3rd most abundant element at ranging from 16 to 20 percent but was not different between groups. Aluminum was detected on each construct surface ranging from 2.1 to 4.9 percent. Phosphate was detected on Biomimetic architectures only and was the least present element (Table 2).

Mechanical properties were affected by construct geometry and HIP treatment.

Bulk mechanical properties differed between the two types of constructs. Mechanical testing to construct failure demonstrated distinct differences due to geometry. Compressive modulus was higher in the biomimetic constructs compared to the geometric constructs, and HIP treatment did not affect compressive modulus for either group (Fig. 3a). Biomimetic constructs also possessed greater toughness and were able to sustain more load and maintain ductility versus their simple cubic counterparts (Fig. 3b). Biomimetic constructs independent of HIP treatment sustained loads of 18kN (Fig. 3c), which was higher than the 8kN sustained by the geometric constructs (Fig. 3c).

In contrast to the bulk mechanical properties, construct geometry and HIP treatment affected the fatigue properties. As indicated in the stress-strain curves, the yield region for the biomimetic constructs was much larger than the geometric constructs (Fig. 3d). The failure profile for HIP treated geometric constructs was more abrupt than for its non-HIP treated counterpart (Fig. 3d). Both geometric constructs failed before 0.2 strain whereas biomimetic constructs experienced failure around 0.4 strain (Fig. 3d).

HIP treatment alters the effects of post-build surface treatment.

Previous studies have not examined the effects of post-build HIP treatment on clinically used implant surface properties in the context of cellular response. Following HIP treatment constructs were grit-blasted and acid-etched and compared to non-HIP treated constructs that underwent the same surface treatments. Surface physical properties, a measure of the effectiveness of the grit-blasting, were assessed by confocal laser microscopy and showed that HIP treatment affects manufactured constructs in an architectural dependent manner. The biomimetic constructs deceased average construct microroughness when grit-blasted and acid-etched after HIP treatment (Fig. 4a). In contrast, surface roughness was unchanged for constructs with organized geometric architecture (Fig. 4a). Peak to valley distance was no different across all groups (Fig. 4b). Skewness values, the measure of distribution of peaks or valleys across a flat surface were all positive, showing a surface with peaks protruding from the surface (Fig. 4c). HIP treatment increased skewness compared to non-HIP treated constructs (Fig. 4c). Kurtosis is the measurement of the sharpness of each peak and all groups possessed a kurtosis greater than 4, which demonstrates sharpness of the peaks rather than curved peaks (Fig. 4d).

Topological characteristics of HIP constructs with and without HIP treatment were further assessed by scanning electron microscopy (SEM) to compare roughness at the macro/micro/nanoscale. Surface morphology at the sub-micron and nanoscale are analyzed to assess the effect of acid-etching on surface topography. Constructs were imaged at 35X, 20,000X, and 100,000X magnifications. Macro-scale SEMs were similar to the 3D microCT reconstructions (Fig. 1, Fig. 5). Surface topography was similar across all constructs at the micro and nanoscale independent of HIP treatment or geometry (Fig. 5).

Biological response of MSCs to surface topography varied with construct architecture and surface topography.

Successful osseointegration depends on a complex microenvironment governed by osteoblast-lineage cells. Therefore, the ability for an implantable material to direct cellular response and enhance osteogenic protein production will increase net bone formation *in vivo*.[31] Previous research has demonstrated the ability for Ti surface treatments to enhance osteoblast response and direct MSC differentiation into osteoblasts without exogenous factors in the culture medium.[31–33] MSCs undergo rapid differentiation on microstructured Ti and Ti6Al4V surfaces, exhibiting osteoblast properties within 7 days of culture in growth media. Accordingly, MSCs were cultured for 7 days on the biomimetic and geometric constructs that were fabricated with and without HIP treatment. All constructs were processed post-build and HIP treatment by grit blasting and acid etching to generate a micro/meso/nano topography.

HIP treatment did not affect total DNA content (Fig. 5a). However, constructs with the biomimetic architecture had decreased DNA content compared to HIP treated geometric constructs. Alkaline phosphatase specific activity in the cell layer lysate was deceased on biomimetic 3D constructs compared to HIP treated geometric constructs, and alkaline phosphatase activity was only increased in the organized geometric constructs treated by HIP (Fig. 5b).

Osteocalcin (OCN), a late differentiation marker for osteoblasts [34], was increased on biomimetic constructs compared to geometric constructs of matching HIP status (Fig. 5c). Autocrine/paracrine signaling proteins BMP2 and VEGF were quantified in the conditioned media as indicators of osteoblast differentiation. BMP2 was not affected by HIP treatment. However, BMP2 production was decreased on HIP treated geometric constructs compared to both biomimetic groups. Biomimetic constructs produced more VEGF than geometric constructs, and post-treatment by HIP showed no differences in VEGF production within architectural groupings (Fig. 5e). The production of the osteoclast modulatory protein, osteoprotegerin (OPG), was more robust on biomimetic constructs compared to HIP geometric and HIP treatment did not affect this production (Fig. 5f).

Cytokines interleukin 6 (IL6) and 10 (IL10) were assessed to determine the immunomodulatory profile of MSCs cultured in these 3D AM constructs. IL6, a regulator of osteoclast precursors [35], was elevated on the biomimetic constructs and was not altered by HIP treatment (Fig. 5g). IL10, a potent anti-inflammatory cytokine, was unchanged between all groups regardless of construct architecture or HIP treatment (Fig. 5h).

Discussion

This study demonstrates that the material processing effects of HIP treatment are highly dependent on the 3D architecture of an AM implant. These material processing differences after HIP treatment of the bulk implant alter necessary post-manufacturing modifications of the implant surface. Most importantly for 3D AM orthopaedic and dental implants, HIP treatment may differentially affect the biological response of cells depending on the porous architecture selected during implant design.

Architecture contributes to mechanical resistance to loading.[36] Mechanical testing of the four construct groups demonstrated increased toughness and ductility in the biomimetic constructs. These properties are most likely due to the decreased strut thickness and increased strut distribution, resulting in an increased ability to transfer loads throughout the construct and increased fatigue resistance. These results are supported by studies using unit cell design alterations to predict mechanical properties of macroporous constructs. In these studies, randomization increases compressive strength and post-build heat treatments are capable of improving fatigue life.[37] Future mechanical analyses of these constructs will examine the response of these biomimetic constructs to fatigue testing.

The cube-like lattice structure in the geometric constructs was unable to transfer load as efficiently as the biomimetic constructs, reducing their ductility. Moreover, HIP treatment further reduced the ductility of geometric constructs resulting in a brittle-like fracture. HIP treatment fuses microvoids and spaces between fused particles produced during the build process.[37,38] The reduction in ductility observed in the present study, therefore, was most likely due to decreased void space for dislocations to move in response to loading, resulting in stress concentrations, crack formation, and sudden failure.

HIP treatment did not affect macroscale construct architecture, which is understandable since the action of HIP treatment is at the submicron level.[38] Our findings suggest that manufacturing parameters together with design architecture may determine the effectiveness of HIP treatment on construct mechanical properties; demonstrated by decreased closed porosity on HIP treated biomimetic constructs compared to their untreated controls and no difference between geometric constructs regardless of HIP treatment. Therefore, HIP treatment may be more effective in cases where numerous fusion site discontinuities are created during the fabrication process and in cases of irregular porosities or architectures commonly associated with complex designs. Studies are needed to test the effects of varying laser scan speed, laser power, and HIP temperature and treatment duration on construct response.

Surface topography is an important regulator of cellular response during osseointegration, demonstrated by increased bone-to-implant contact with increasing microroughness.[39,40] Interestingly, HIP treatment was shown to impact the outcomes of post-manufacturing modifications, demonstrated by decreased microroughness on the HIP treated biomimetic constructs and increased skewness of the surface microstructures on HIP treated constructs of both architectures.

This effect on the outcome of surface treatment can vary with construct architecture and surface area available for grit-blasting.[41] HIP treatment likely reduces the effectiveness of physical methods to induce surface roughness by increasing the localized hardness of the construct surfaces. In contrast, chemical processes like acid-etching are unaffected, shown by similar sub-micron and nanoscale topography. HIP treatment did not affect either bulk chemistry or surface chemistry of the constructs. EDX showed decreased weight percentage of vanadium in the bulk material, and vanadium was not detectable by XPS on the implant surface. This suggests that there was preferential etching of vanadium rich areas of the fused Ti6Al4V particles. Phosphate was detected on the surface of biomimetic groups by XPS, which was not a surprising finding given that the grit-blasting material was calcium phosphate and particles could have been trapped due to the irregular architecture.

No differences were detected by EDX or XPS between the constructs with respect to percent element composition. This suggests that the cellular response to complex architectures was not mediated by the chemical composition, either of the bulk material or of the surface. Although there were differences in microroughness of biomimetic constructs with and without-HIP treatment, cell responses were similar, suggesting that sub-micron and nanoscale topography may have a greater influence than overall average microroughness. Previous studies demonstrated that MSCs are sensitive to kurtosis and skewness of Ti6Al4V surfaces, even when average roughness is comparable [14], and both of these properties were affected by HIP. Studies have also shown that HIP treatment of Ti6Al4V without removing the diffusion layer (150 μm) can reduce the fatigue properties of the metal due to stress concentrations, and processing to remove the diffusion layer can increase fatigue properties.[42] Therefore post-processing with grit-blasting and acid-etching in the present study can also be mechanically beneficial for HIP treated Ti and will be investigated further.

Pore size and porosity have been shown to alter the degree of osseointegration of porous implants *in vivo* and *in vitro* cellular response. Studies examining varying pore sizes in AM femoral bone defect implants in goats demonstrated an ability for cells to infiltrate and produce new bone at 300 to 400 μm, while other studies in rabbits have shown that 600 μm pore size enhances osseointegration compared to 300 and 900 μm.[23,43] These variabilities in outcomes suggest other factors contribute to the osseointegration of a porous implant.

Recent studies comparing porous constructs and solid implants, both with clinically relevant surface treatments showed comparable mechanical force to failure even though porous implants had bone ingrowth whereas solid implants had bone on-growth.[22,44,45] These earlier studies did not examine the effects of differing porous architecture while maintaining pore size and porosity. Here we show that geometric cues outside of pore size and porosity contribute to the osteoblastic response of MSCs over seven days. Compared to the geometric construct, the biomimetic construct architecture, which is similar to trabecular bone enhanced osteoblastic response as shown by increased production of osteocalcin, a late-stage osteoid protein that regulates mineralization; the osteoclast differentiation and activation inhibitor osteoprotegerin [46–48]; and the potent angiogenesis protein, VEGF-A.[10,12,32]

Cytokines IL6 and IL10 are important regulators of immune response.[49,50] Recent studies have shown that in addition to being a pro-inflammatory cytokine, IL6 decreases membrane

expression of receptor activator of NF-κB (RANK) in pre-osteoclasts, preventing osteoclast differentiation. Cells cultured on biomimetic constructs produced more IL6. Together with increased production of TGF-β1 super family proteins and osteoprotegerin, our findings suggest that these cells may be downregulating osteoclast populations.[35] IL10 is a potent anti-inflammatory marker and is expressed equally between all constructs and to a greater extent than IL6, creating a favorable microenvironment for MSC differentiation and osteoblast maturation.[51]

Extensive research has been conducted and summarized on the subject of biomimetic materials, topographies, and architecture and targeted cellular response.[9,18,52] In the context of osseointegration, the biomimetic construct groups possess both biomimetic surface topography and biomimetic architecture, while geometric constructs only possess biomimetic surface topography. This biomimetic surface topography resembles osteoclast resorption pits and has been shown to increase osteoblast maturation and response. The addition of biomimetic architecture most likely contributes through altered cytoskeletal reorganization that activates signaling pathways which increase osteoblast response. Previous studies have shown that cytoskeletal reorganization in response to implant surface or cell spanning of pores results in increased production of osteoblast markers. [23,53,54]

Ti6Al4V constructs produced by AM and processed by HIP treatment support the ability of MSCs to produce equivalent concentrations of soluble signaling proteins compared to non-treated AM constructs. These signaling proteins are necessary for osteoblastic differentiation of MSCs within the implant micro-environment. Therefore we suggest that the post-manufacturing modification by HIP treatment does not significantly alter cellular response and could be a viable option to increase the mechanical longevity of AM constructs.

Conclusion

In summary, osseointegration is a complex cascade of biological events known to be influenced by implant chemistry and surface properties. These data demonstrate that implant architecture influences cellular response and biomimetic architecture increases production of osteogenic factors. Moreover, these data demonstrate that Ti-based constructs can be treated by hot isostatic pressure to improve construct longevity, while not diminishing the ultimate construct mechanical properties or disrupting the response of MSCs on the implant surface when manufactured constructs are subsequently modified by grit-blasting and acid-etching. However, HIP treatment can reduce the efficiency of physical surface treatments such as grit-blasting, which can alter the surface properties of implants treated by HIP; therefore, implants modified after HIP treatment should be characterized to ensure the implant surface is still favorable for bone apposition.

Acknowledgements

AB Dental (Ashdod, Israel) provided the surfaces and support for this study. The National Institute of Arthritis and Musculoskeletal and Skin Diseases of the National Institutes of Health under Award Numbers R01AR052102 and R01AR072500 provided additional support.

Disclosures:

BDB is a consultant for Institut Straumann AG (Basel, Switzerland) and Titan Spine LLC (Mequon, WI). This study was funded in part by AB Dental.

References

1. Guobis Z, Pacauskiene I, Astramskaite I. General Diseases Influence on Peri-Implantitis Development: a Systematic Review. J Oral Maxillofac Res 2016;7:1–16. 10.5037/jomr.2016.7305.
2. Turri A, Rossetti P, Canullo L, Grusovin M, Dahlin C. Prevalence of Peri-implantitis in Medically Compromised Patients and Smokers: A Systematic Review. Int J Oral Maxillofac Implants 2016;31:111–8. 10.11607/jomi.4149. [PubMed: 26800167]
3. Reginster JY, Burlet N. Osteoporosis: A still increasing prevalence. Bone 2006;38:1998–2003. 10.1016/j.bone.2005.11.024.
4. Burge R, Dawson-Hughes B, Solomon DH, Wong JB, King A, Tosteson A. Incidence and economic burden of osteoporosis-related fractures in the United States, 2005–2025. J Bone Miner Res 2007;22:465–75. 10.1359/jbmr.061113. [PubMed: 17144789]
5. Barfeie A, Wilson J, Rees J. Implant surface characteristics and their effect on osseointegration. Br Dent J 2015;218:1–9. 10.1038/sj.bdj.2015.171. [PubMed: 25571796]
6. Cheng A, Goodwin WB, deGlee BM, Gittens RA, Vernon JP, Hyzy SL, et al. Surface modification of bulk titanium substrates for biomedical applications via low-temperature microwave hydrothermal oxidation. J Biomed Mater Res A 2017 10.1002/jbm.a.36280.
7. Zhao G, Schwartz Z, Wieland M, Rupp F, Geis-Gerstorfer J, Cochran DL, et al. High surface energy enhances cell response to titanium substrate microstructure. J Biomed Mater Res - Part A 2005;74:49–58. 10.1002/jbm.a.30320.
8. Gittens R a., Scheideler L, Rupp F, Hyzy SL, Geis-Gerstorfer J, Schwartz Z, et al. A review on the wettability of dental implant surfaces II: Biological and clinical aspects. Acta Biomater 2014;10:2907–18. 10.1016/j.actbio.2014.03.032. [PubMed: 24709541]
9. Boyan BD, Lotz EM, Schwartz Z. (*) Roughness and Hydrophilicity as Osteogenic Biomimetic Surface Properties. Tissue Eng Part A 2017;23:1479–89. 10.1089/ten.TEA.2017.0048. [PubMed: 28793839]
10. Boyan BD, Lossdörfer S, Wang L, Zhao G, Lohmann CH, Cochran DL, et al. Osteoblasts generate an osteogenic microenvironment when grown on surfaces with rough microtopographies. Eur Cells Mater 2003;6:22–7. https://doi.org/vol006a03 [pii].
11. Olivares-Navarrete R, Hyzy SL, Haithcock DA, Cundiff CA, Schwartz Z, Boyan BD. Coordinated regulation of mesenchymal stem cell differentiation on microstructured titanium surfaces by endogenous bone morphogenetic proteins. Bone 2015;73:208–16. 10.1016/j.bone.2014.12.057. [PubMed: 25554602]
12. Raines AL, Olivares-Navarrete R, Wieland M, Cochran DL, Schwartz Z, Boyan BD. Regulation of angiogenesis during osseointegration by titanium surface microstructure and energy. Biomaterials 2010;31:4909–17. 10.1016/j.biomaterials.2010.02.071. [PubMed: 20356623]
13. Olivares-Navarrete R, Hyzy SL, Hutton DL, Erdman CP, Wieland M, Boyan BD, et al. Direct and indirect effects of microstructured titanium substrates on the induction of mesenchymal stem cell differentiation towards the osteoblast lineage. Biomaterials 2010;31:2728–35. 10.1016/j.biomaterials.2009.12.029. [PubMed: 20053436]
14. Olivares-Navarrete R, Hyzy SL, Berg ME, Schneider JM, Hotchkiss K, Schwartz Z, et al. Osteoblast Lineage Cells Can Discriminate Microscale Topographic Features on Titanium-Aluminum-Vanadium Surfaces. Ann Biomed Eng 2014;42:2551–61. 10.1007/s10439-014-1108-3. [PubMed: 25227453]
15. Olivares-Navarrete R, Hyzy SL, Gittens RA, Schneider JM, Haithcock D, Ullrich P, et al. Rough Titanium Alloys Regulate Osteoblast Production of Angiogenic Factors. Spine J 2013;13:10.1016/j.spinee.2013.03.047 . 10.1016/j.spinee.2013.03.047https://doi.org/10.1016/j.spinee.2013.03.047. https://doi.org/10.1016/j.spinee.2013.03.047 .
16. Girasole G, Muro G, Mintz A, Chertoff J. Transforaminal lumbar interbody fusion rates in patients using a novel titanium implant and demineralized cancellous allograft bone sponge. Int J Spine Surg 2013;7:e95–100. 10.1016/j.ijsp.2013.08.001. [PubMed: 25580378]

17. Sing SL, An J, Yeong WY, Wiria FE. Laser and electron-beam powder-bed additive manufacturing of metallic implants: A review on processes, materials and designs. J Orthop Res 2016;34:369–85. 10.1002/jor.23075. [PubMed: 26488900]

18. Wang X, Xu S, Zhou S, Xu W, Leary M, Choong P, et al. Topological design and additive manufacturing of porous metals for bone scaffolds and orthopaedic implants: A review. Biomaterials 2016;83:127–41. 10.1016/j.biomaterials.2016.01.012. [PubMed: 26773669]

19. Cheng A, Humayun A, Cohen DJ, Boyan BD, Schwartz Z. Additively manufactured 3D porous Ti-6Al-4V constructs mimic trabecular bone structure and regulate osteoblast proliferation, differentiation and local factor production in a porosity and surface roughness dependent manner. Biofabrication 2014;6:045007 10.1088/1758-5082/6/4/045007. [PubMed: 25287305]

20. Wieding J, Wolf A, Bader R. Numerical optimization of open-porous bone scaffold structures to match the elastic properties of human cortical bone. J Mech Behav Biomed Mater 2014;37:56–68. 10.1016/j.jmbbm.2014.05.002. [PubMed: 24942627]

21. Cheng A, Cohen DJ, Kahn A, Clohessy RM, Sahingur K, Newton JB, et al. Laser Sintered Porous Ti–6Al–4V Implants Stimulate Vertical Bone Growth. Ann Biomed Eng 2017;45:2025–35. 10.1007/s10439-017-1831-7. [PubMed: 28409291]

22. Hyzy SL, Cheng A, Cohen DJ, Yatzkaier G, Whitehead AJ, Clohessy RM, et al. Novel hydrophilic nanostructured microtexture on direct metal laser sintered Ti–6Al–4V surfaces enhances osteoblast response in vitro and osseointegration in a rabbit model. J Biomed Mater Res - Part A 2016;104:2086–98. 10.1002/jbm.a.35739.

23. Li G, Wang L, Pan W, Yang F, Jiang W, Wu X, et al. In vitro and in vivo study of additive manufactured porous Ti6Al4V scaffolds for repairing bone defects. Sci Rep 2016;6:1–11. 10.1038/srep34072. [PubMed: 28442746]

24. Dallago M, Fontanari V, Torresani E, Leoni M, Pederzolli C, Potrich C, et al. Journal of the Mechanical Behavior of Biomedical Materials Fatigue and biological properties of Ti-6Al-4V ELI cellular structures with variously arranged cubic cells made by selective laser melting. J Mech Behav Biomed Mater 2018;78:381–94. 10.1016/j.jmbbm.2017.11.044. [PubMed: 29220822]

25. Benedetti M, Torresani E, Leoni M, Fontanari V, Bandini M, Pederzolli C, et al. Journal of the Mechanical Behavior of Biomedical Materials The effect of post-sintering treatments on the fatigue and biological behavior of Ti-6Al-4V ELI parts made by selective laser melting. J Mech Behav Biomed Mater 2017;71:295–306. 10.1016/j.jmbbm.2017.03.024. [PubMed: 28376363]

26. Makes A, Collaborative AAMS. Standardization Roadmap for Additive Manufacturing - Version 2.0. vol. 2 2018.

27. Xu L, Guo R, Bai C, Lei J, Yang R. Effect of Hot Isostatic Pressing Conditions and Cooling Rate on Microstructure and Properties of Ti-6Al-4V Alloy from Atomized Powder. J Mater Sci Technol 2014;30:1289–95. 10.1016/j.jmst.2014.04.011.

28. Zhang K, Mei J, Wain N, Wu X. Effect of hot-isostatic-pressing parameters on the microstructure and properties of powder Ti-6Al-4V hot-isostatically-pressed samples. Metall Mater Trans A Phys Metall Mater Sci 2010;41:1033–45. 10.1007/s11661-009-0149-y.

29. Alrabeah GO, Brett P, Knowles JC, Petridis H. The effect of metal ions released from different dental implant-abutment couples on osteoblast function and secretion of bone resorbing mediators. J Dent 2017;66:91–101. [PubMed: 28800964]

30. Cheng A, Cohen DJ, Boyan BD, Schwartz Z. Laser-Sintered Constructs with Bioinspired Porosity and Surface Micro/Nano-Roughness Enhance Mesenchymal Stem Cell Differentiation and Matrix Mineralization In Vitro. Calcif Tissue Int 2016;99:625–37. 10.1007/s00223-016-0184-9. [PubMed: 27501817]

31. Wennerberg A, Albrektsson T. Effects of titanium surface topography on bone integration: A systematic review. Clin Oral Implants Res 2009;20:172–84. 10.1111/j.1600-0501.2009.01775.x. [PubMed: 19663964]

32. Olivares-Navarrete R, Raines AL, Hyzy SL, Park JH, Hutton DL, Cochran DL, et al. Osteoblast maturation and new bone formation in response to titanium implant surface features are reduced with age. J Bone Miner Res 2012;27:1773–83. 10.1002/jbmr.1628. [PubMed: 22492532]

33. Olivares-Navarrete R, Raz P, Zhao G, Chen J, Wieland M, Cochran DL, et al. Integrin alpha2beta1 plays a critical role in osteoblast response to micron-scale surface structure and surface energy of

titanium substrates. Proc Natl Acad Sci U S A 2008;105:15767–72. 10.1073/pnas.0805420105. [PubMed: 18843104]

34. Hall BK. Chapter 24 - Osteoblast and Osteocyte Diversity and Osteogenesis In Vitro In: Hall BKBT-B and C (Second E, editor San Diego: Academic Press; 2015 p. 401–13.
35. Yoshitake F, Itoh S, Narita H, Ishihara K, Ebisu S. Interleukin-6 directly inhibits osteoclast differentiation by suppressing receptor activator of NF-??B signaling pathways. J Biol Chem 2008;283:11535–40. 10.1074/jbc.M607999200. [PubMed: 18296709]
36. Wegst UGK, Bai H, Saiz E, Tomsia AP, Ritchie RO. Bioinspired structural materials. Nat Mater 2015;14:23–36. 10.1038/NMAT4089. [PubMed: 25344782]
37. Mullen L, Stamp RC, Fox P, Jones E, Ngo C, Sutcliffe CJ. Selective laser melting: A unit cell approach for the manufacture of porous, titanium, bone in-growth constructs, suitable for orthopedic applications. II. Randomized structures. J Biomed Mater Res - Part B Appl Biomater 2010;92:178–88. 10.1002/jbm.b.31504. [PubMed: 19810111]
38. Atkinson HV, Davies S. Fundamental Aspects of Hot Isostatic Pressing : An Overview. Metall Mater Trans A Phys Metall Mater Sci 2000;m:
39. Buser D, Schenk RK, Steinemann S, Fiorellini JP, Fox CH, Stich H. Influence of surface characteristics on bone integration of titanium implants. A histomorphometric study in miniature pigs. J Biomed Mater Res 2018;25:889–902. 10.1002/jbm.820250708.
40. Buser D, Janner SFM, Wittneben J, Brägger U, Ramseier CA, Salvi GE. 10-Year Survival and Success Rates of 511 Titanium Implants with a Sandblasted and Acid-Etched Surface : A Retrospective Study in 303 Partially. Clin Oral Implants Res 2012;26:1121–8. 10.1111/j.1708-8208.2012.00456.x.
41. Le Guéhennec L, Soueidan A, Layrolle P, Amouriq Y. Surface treatments of titanium dental implants for rapid osseointegration. Dent Mater 2007;23:844–54. 10.1016/j.dental.2006.06.025. [PubMed: 16904738]
42. Davidson a., Zhang K, Yuan W, Mei J, Hurley P, Bache MR, et al. Influence of surface layer on properties of hipped Ti–6Al–4V. Mater Sci Technol 2006;22:553–60. 10.1179/174328406X84085.
43. Taniguchi N, Fujibayashi S, Takemoto M, Sasaki K, Otsuki B, Nakamura T, et al. Effect of pore size on bone ingrowth into porous titanium implants fabricated by additive manufacturing: An in vivo experiment. Mater Sci Eng C 2016;59:690–701. 10.1016/j.msec.2015.10.069.
44. Cheng A, Humayun A, Cohen DJ. Performance of laser sintered Ti – 6Al – 4V implants with bone-inspired porosity and micro / nanoscale surface roughness in the rabbit femur. Biomed Mater 2017;12:25021.
45. Cheng A, Humayun A, Boyan BD, Schwartz Z. Enhanced Osteoblast Response to Porosity and Resolution of Additively Manufactured Ti-6Al-4V Constructs with Trabeculae-Inspired Porosity. 3D Print Addit Manuf 2016;3:10–21. 10.1089/3dp.2015.0038. [PubMed: 28804735]
46. Boyce BF, Xing L. The RANKL/RANK/OPG pathway. Curr Osteoporos Rep 2007;5:98–104. 10.1007/s11914-007-0024-y. [PubMed: 17925190]
47. Lossdörfer S, Schwartz Z, Wang L, Lohmann CH, Turner JD, Wieland M, et al. Microrough implant surface topographies increase osteogenesis by reducing osteoclast formation and activity. J Biomed Mater Res Part A 2004;70A:361–9. 10.1002/jbm.a.30025.
48. Lotz EM, Berger MB, Schwartz Z, Boyan BD. Regulation of osteoclasts by osteoblast lineage cells depends on titanium implant surface properties. Acta Biomater 2018;68:296–307. 10.1016/j.actbio.2017.12.039. [PubMed: 29292169]
49. Schwartz Z, Lohmann CH, Sisk M, Cochran DL, Sylvia VL, Simpson J, et al. Local factor production by MG63 osteoblast-like cells in response to surface roughness and 1,25-(OH)2D3 is mediated via protein kinase C- and protein kinase A-dependent pathways. Biomaterials 2001;22:731–41. [PubMed: 11246968]
50. Hyzy SL, Olivares-Navarrete R, Hutton DL, Tan C, Boyan BD, Schwartz Z. Microstructured titanium regulates interleukin production by osteoblasts, an effect modulated by exogenous BMP-2. Acta Biomater 2013;9:5821–9. 10.1016/j.actbio.2012.10.030. [PubMed: 23123301]
51. Hotchkiss KM, Reddy GB, Hyzy SL, Schwartz Z, Boyan BD, Olivares-Navarrete R. Titanium surface characteristics, including topography and wettability, alter macrophage activation. Acta Biomater 2016;31:425–34. 10.1016/j.actbio.2015.12.003. [PubMed: 26675126]

52. Raghavendra S, Wood MC, Taylor TD, Raghavendra S Taylor TD, WMC, Raghavendra S, Wood MC, et al. Early wound healing around endosseous implants: a review of the literature. Int J Oral Maxillofac Implants 2005;20:425–31. 10.1016/S0084-3717(08)70105-3. [PubMed: 15973954]

53. Lai M, Hermann CD, Cheng A, Olivares-Navarrete R, Gittens RA, Bird MM, et al. Role of A2B1 integrins in mediating cell shape on microtextured titanium surfaces. J Biomed Mater Res - Part A 2015;103:564–73. 10.1002/jbm.a.35185.

54. Lo Y-P, Liu Y-S, Rimando MG, Ho JH-C, Lin K, Lee OK. Three-dimensional spherical spatial boundary conditions differentially regulate osteogenic differentiation of mesenchymal stromal cells. Sci Rep 2016;6:21253 10.1038/srep21253. [PubMed: 26884253]

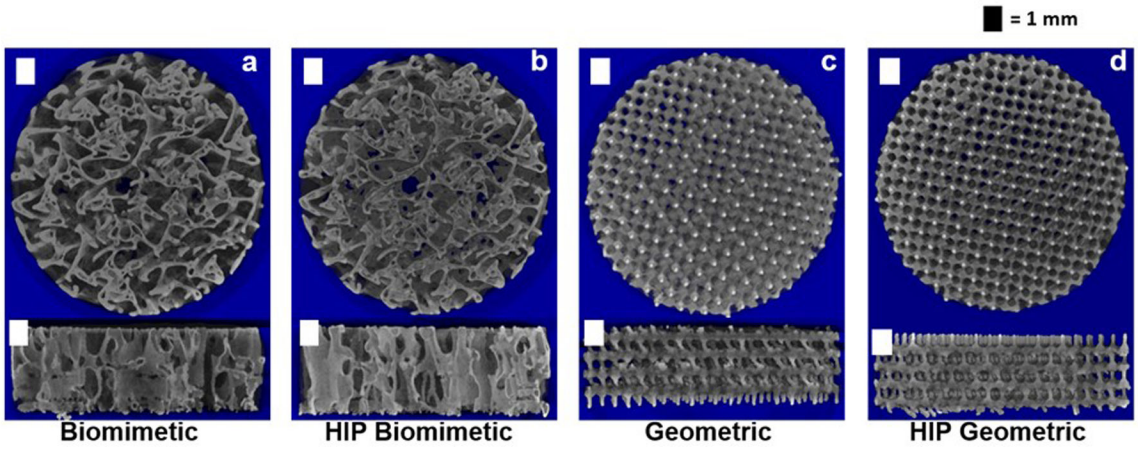

Figure 1.

Additive manufacturing is capable of producing constructs with consistent geometry. 3D reconstructions of microCT scans of Biomimetic (a, b) and Geometric (c, d) additively manufactured constructs without (a, c) or with hot isostatic pressure (HIP) treatment (b, d). Scale bar is 1 mm.

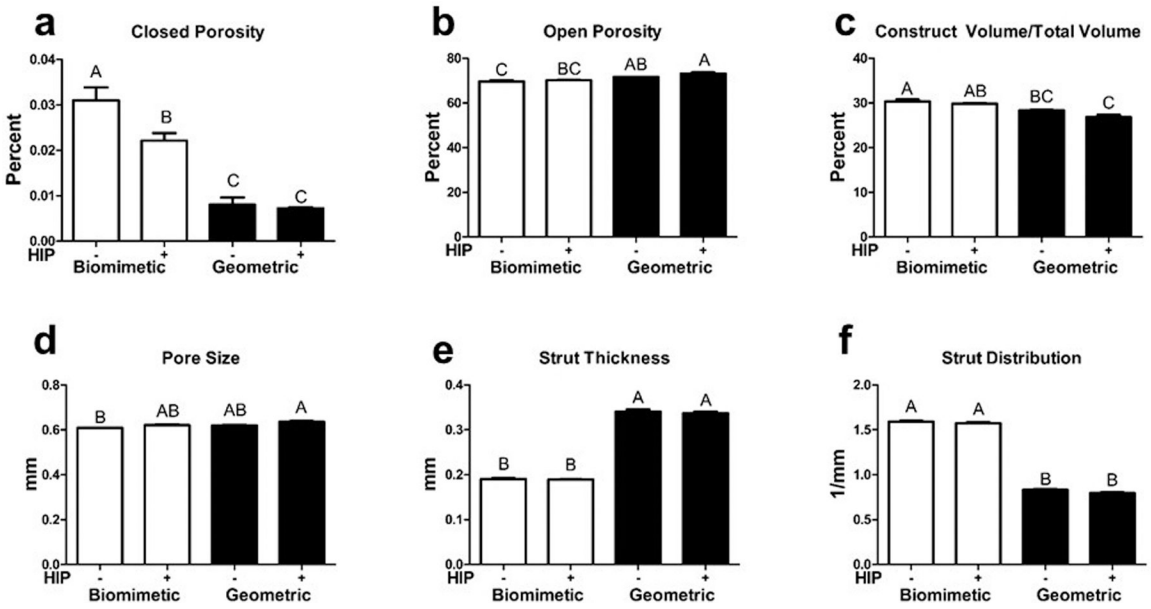

Figure 2.

HIP treatment does not alter pore size and porosity. Quantification of microCT scans taken of Biomimetic and Geometric constructs having undergone HIP treatment. Closed (a) and Open (b) Porosity, Construct volume/Total Volume (c), Pore Size (d), Strut Thickness (e), Strut Distribution (f) were assessed. Strut distribution is a mean measurement of distance from mid-axes determined in the void spaces of each construct and serves as a quantification of the number of struts within a unit volume of each construct. Groups not sharing letters are significantly different at a $p<0.05$; $n = 3$ per group.

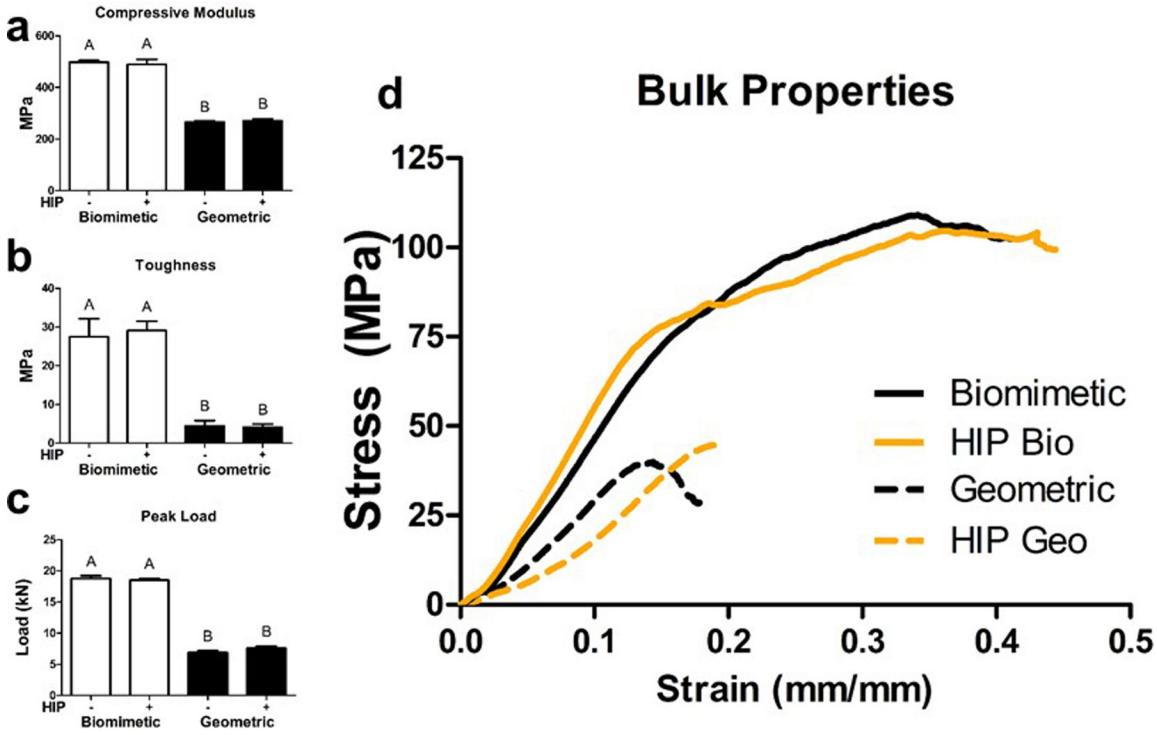

Figure 3.

Bulk mechanical properties of 3-dimensional additively manufactured constructs. Constructs were assessed for compressive modulus (a), toughness (b), and peak sustained Load (c) by an electromechanical testing apparatus to determine the effects of geometry and HIP treatment on construct properties. Stress-strain curve for all four groups (d). Shown are HIP treated constructs in gold and non-treated are in black. Solid lines denote biomimetic constructs and dash lines represent geometric constructs. Groups not sharing letters are significantly different at a $p<0.05$; $n = 6$ per group.

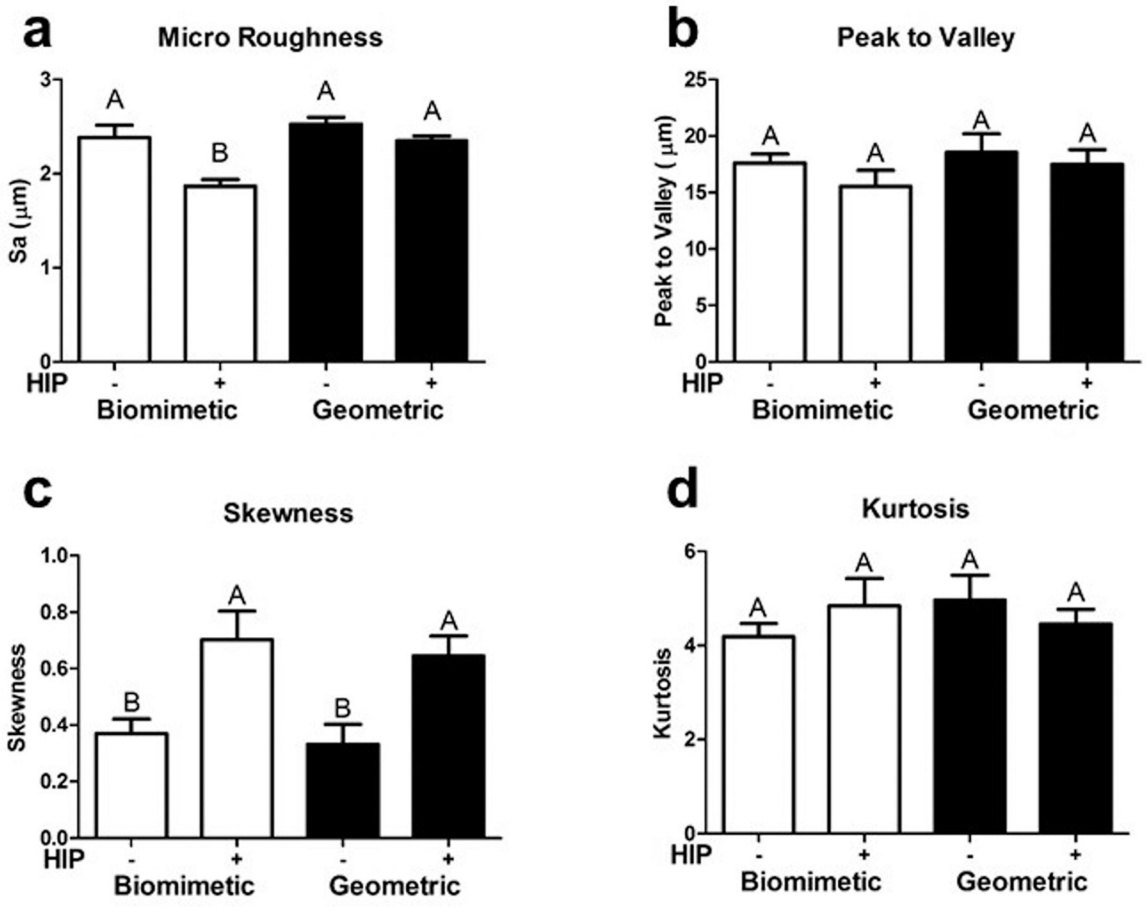

Figure 4.

Quantification of surface properties of additively manufactured constructs by confocal laser microscopy. Optical profilometry was used to assess average surface microroughness (a), peak to valley distance (b), skewness (c) and kurtosis (d) on constructs following grit-blasting and acid-etching. Groups not sharing letters are significantly different at a $p<0.05$; n = 5 per construct and two constructs per group.

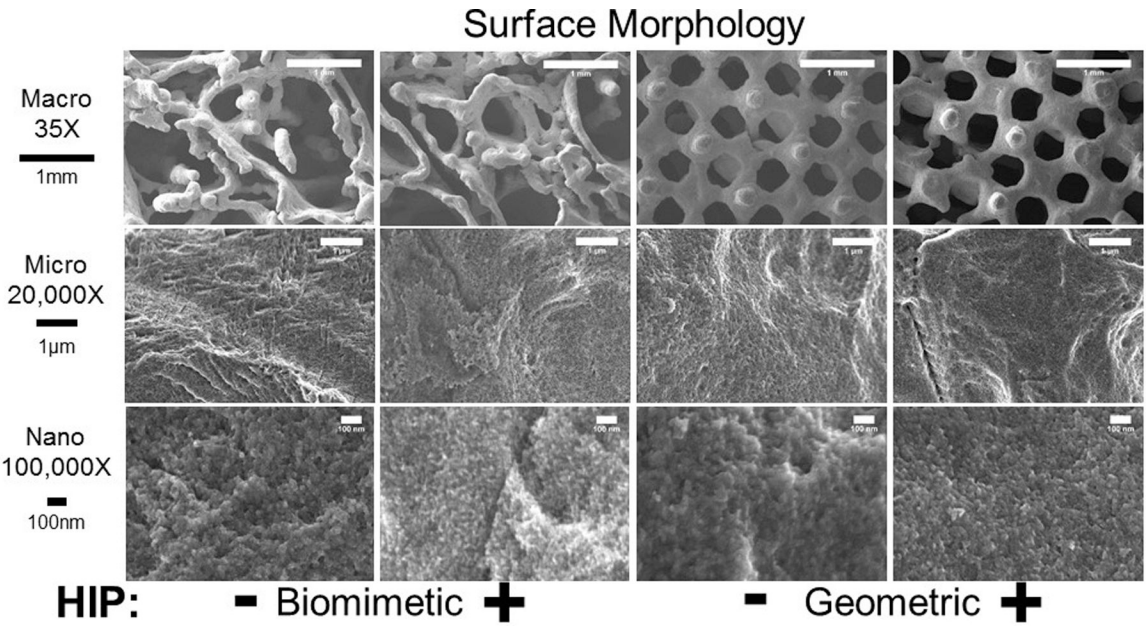

Figure 5.

Characterization of surface morphology using scanning electron microscopy. Surface morphology at the sub-micron and nanoscale are analyzed to assess the effect of acid-etching on surface topography. Constructs were imaged at 35X, 20,000X, and 100,000X magnifications. Macro images scale bar are 1 mm, micro images have a scale bar of 1 μm, and nanoscale images have a scale bar of 100 nm.

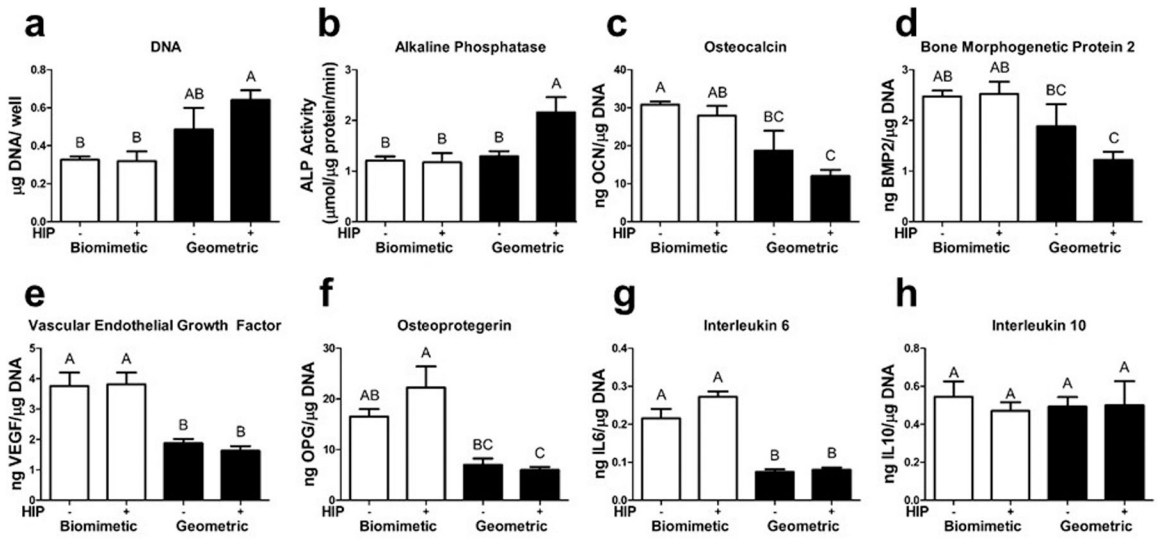

Figure 6.

Assessment of biologic response to 3D additively manufactured constructs having undergone HIP treatment. MSCs were cultured on biomimetic and organized geometric AM constructs for seven days and assessed for osteogenic markers. Total DNA content (a) and alkaline phosphatase specific activity (b) were determined in the cell lysate. Osteogenic markers osteocalcin (c), bone morphogenetic protein 2 (BMP2, d), vascular endothelial growth factor (VEGF, e), osteoprotegerin (OPG, f) and cytokines interleukin 6 (IL6, g) and 10 (IL10, h) were quantified in cell supernatant. Groups not sharing letters are significantly different at a $p<0.05$; $n = 6$ per group.

Table 1.

Bulk Chemistry (EDX): weight % average

EDX	Biomimetic	HIP Biomimetic	Geometric	HIP Geometric
Titanium	90.7 ± 0.7	91.2 ± 0.5	89.9 ± 0.4	91.0 ± 0.6
Aluminum	8.1 ± 0.5	7.8 ± 0.4	7.5 ± 0.3	8.0 ± 0.5
Vanadium	1.2 ± 0.8	1.0 ± 0.6	1.6 ± 0.8	1.0 ± 0.7

Table 2.

Surface Chemistry (XPS): atomic % average

XPS	Biomimetic	HIP Biomimetic	Geometric	HIP Geometric
Titanium	16.1 ± 0.8	17.1 ± 1.5	19.0 ± 0.3	20.1 ± 0.8
Aluminum	3.1 ± 0.2	2.1 ± 0.5	3.5 ± 1.1	4.9 ± 0.9
Oxygen	55.6 ± 0.7	56.2 ± 0.9	55.5 ± 1.1	53.4 ± 0.8
Carbon	22.9 ± 1.2	22.2 ± 2.2	22.0 ± 0.4	21.9 ± 1.6
Phosphate	2.1 ± 0.7	2.6 ± 0.7	-	-
Vanadium	-	-	-	-